Application of ultrasonic tomography to characterize the mechanical state of standing trees (*Picea abies*)

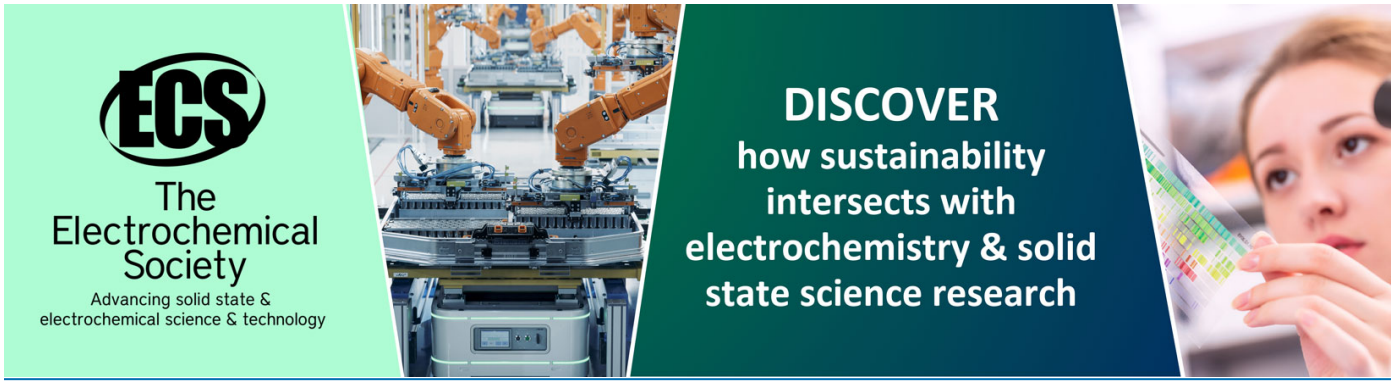

Journal of Physics: Conference Series **353** (2012) 012007 doi:10.1088/1742-6596/353/1/012007

Application of ultrasonic tomography to characterize the mechanical state of standing trees (*Picea abies*)

L Brancheriau[1], A Ghodrati[2], P Gallet[1], P Thaunay[1], P Lasaygues[3]

[1] Production and Processing of Tropical Woods, CIRAD, Montpellier, France
[2] Islamic Azad University, Science and Research Branch, Tehran, Iran
[3] Laboratory of Mechanics and Acoustics, UPR CNRS 7051, Marseille, France

E-mail: loic.brancheriau@cirad.fr

Abstract. Wood is a biological growth medium. It is orthotropic with longitudinal, radial and tangential axes. Furthermore, standing trees adapt themselves to environmental growth conditions, and their material properties vary with age. These changes result in variations that are much more complex than anisotropy. Studying wood quality and intraspecific variability is useful for clonal selection and for the genetic improvement of plantations. In this study, two logs of *Picea abies* underwent transmission tomography. The mean diameter was 16 cm (26-year-old tree) and the moisture content was 22%. The effect of the presence of bark and artificial defects was investigated. The tomographic device was specifically built for tree imaging. The imaging process was automatic with 900 ultrasonic acquisitions in 40 minutes (emission at 55 kHz with 5 periods of square wave form). The main conclusions were: speed near the bark is higher than in the centre because of the existence of juvenile wood combined with the moisture content gradient (moisture content lower near the bark). Likewise, damping near the bark is lower than in the centre. A significant relationship was observed between slowness and attenuation (R^2=0.50); when the speed increased, damping decreased. No clear effect of the presence of bark was shown on the tomographic images. The bark was thin (3 to 5 mm thick) compared to the wavelength (26 mm). The 10, 20 and 50 mm artificial holes were clearly visible on the tomographic images. However, quantitative tomography does not enable the precise location of defects.

1. Introduction

Wood is a biological end-product generated during cambial growth over successive years [1]. During the growth process, cambium cells convert most photosynthesized products and nutrients into various biopolymers for use in the formation of woody tissues (annual ring and cork formation). Wood can thus be considered as a record of the responses of trees exposed to different growing conditions, but also to changing environments. The properties of an annual ring describe the morphological structure of the species and quantify the reaction of trees to variations in their environment.

In the particular case of plantations, species are usually selected for their fast growth, but the quantity of wood produced does not necessarily mean quality. With a view to improving breeding programmes and genetic selection adapted to new forestry practices, non-destructive techniques need to be directly employed in plantations. The challenge is thus to use accurate techniques capable of quantifying a large number of properties in a few minutes; the apparatus should also be easy to move around the plantation.

The use of elastic waves (ultrasound or sound waves) to detect decay in trees has been explored and reported by many researchers [2, 5, 8, 16]. The concept of detecting decay by this method was initially based on the observation that wave propagation is sensitive to the presence of degradation in wood. In fact, elastic waves appear to travel more slowly in deteriorated wood than they do in normal wood [15]. The first generation of equipment used involved two-probe systems that measured wave TOF in a single path. The suitability of a single-path approach for tree-decay detection has proved to be limited, as stress-wave velocity across tree stems varies substantially even for intact trees, and a standard reference velocity for data interpretation is not readily available [17].

More recently, tomography techniques developed for medical and industrial applications, or geophysical prospecting, have been assessed for their applicability in standing trees. Different imaging techniques were reported by Bucur in 2003 [4]. In that review article, the author detailed the possibilities of using ionizing radiation (X-rays and gamma rays), thermography, microwaves, ultrasonics and nuclear magnetic resonance. A tomograph using ionizing radiation was designed for standing trees [12]. Commercial devices were also developed and were based on determining the time of flight (TOF) of elastic waves induced by an instrumented hammer (acousto-ultrasound tools). These devices were presented in detail by Schubert in 2007 [13]. The three tools were PiCUS®, ARBOTOM® [11] and FAKOPP3D® [7]. In contrast to tomography based on X-rays and gamma-rays, tomographic methods based on electrical resistance, microwaves, or elastic waves are not dangerous. Nicololli [10] compared these three approaches by calculating the tomograms of decayed trunks. These tomographic methods consist in inverting the electrical resistance, or TOF, of electromagnetic and elastic waves by algorithms from the field of geophysics. Tomography based on elastic waves has given the best results in terms of depicting the geometry and location of inner wood-decay. However, times of flight are inverted by filtered back-projection, which assumes isotropic material behaviour and straight rays (PICUS® and FAKOPP3D®). Straight rays are appropriate in isotropic media, otherwise inversion should account for curved rays [6, 14]. Socco (2004) used an iterative TOF inversion method (root mean square optimization method) developed by geophysicists. This inversion method can be used with straight or curved rays [14]. In 2006, Maurer also proposed a correction procedure to take into account the anisotropy of wood. This correction assumed slight anisotropy and took into account a radial to tangential velocity ratio in a standard isotropic reconstruction procedure [9].

With the challenge of using an accurate and fast, non-destructive technique in plantations, the objectives of this study were to design an automatic tomograph and compare how the presence of bark and drilled holes affect the ultrasonic parameters: slowness and attenuation. In the early stages of developing the tomograph, two 300-kHz ultrasonic probes were used [3]. The probes consisted of a wheel in which the emitter was placed, and the coupling medium was formed by an elastomer surrounding the wheel. After several tests on green and dry woods in the transverse and longitudinal directions, those probes were replaced because transmission depth at 300 kHz was between 3 cm and 10 cm, depending on the test configuration (without the presence of bark). The anisotropy of wood was not taken into account and a classic filtered back-projection algorithm was used to compute the tomography maps.

2. Experimental methodology

2.1. Materials

Two spruce (*Picea abies*) logs were harvested from different trees near the city of Nowshahr (Iran). The sampling height was between 0.80 m and 1.30 m. The corresponding mean diameter was between 15.0 cm and 16.5 cm. The cross-section of the logs was almost circular and the logs also had a straight vertical appearance. The trees were 26 years old. Samples were taken in September 2010 and shipped to France to be tested in October; the samples were wrapped in plastic film to minimize the effect of wood drying.

2.2. Experimental protocol

The first log was cut into two 5-cm thick disks and one 15-cm thick disk. The disks were taken from the middle section of the log to avoid cracks due to wood drying, and to have a high moisture content. The 5-cm thick disks were used to determine the mean moisture content, along with the moisture content profile along the radius (figure 1). The moisture content was determined before and after ultrasonic testing. The samples in figure 1 were weighed then dried in an oven (103°C) for 48 hours, then weighed again. Equation 1 was used to compute the moisture content.

$$MC\% = 100\frac{M_H - M_0}{M_0} \quad (1)$$

Where MC is the moisture content, M_H the green weight and M_0 the oven-dry weight.

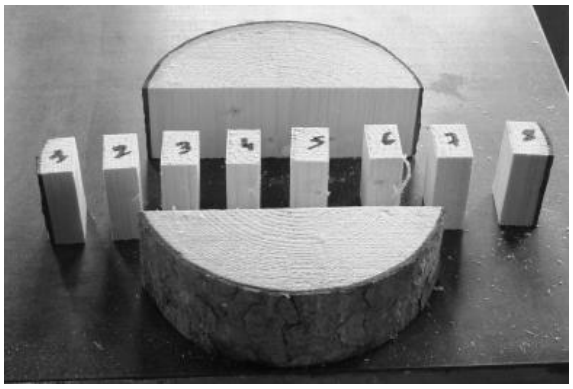

Figure 1. Sampling pattern for moisture content determination (dimensions of the small samples: 2 x 3 x 5 cm^3).

The 15-cm thick disk underwent tomography testing with 3 sample states: with bark, without bark and drilled (2 holes measuring 1 cm and 2 cm in diameter, see figure 2). The tomography tests were carried out with two replications and an angular step of 30° to estimate measurement uncertainties, and with an angular step of 10° for tomographic imaging.

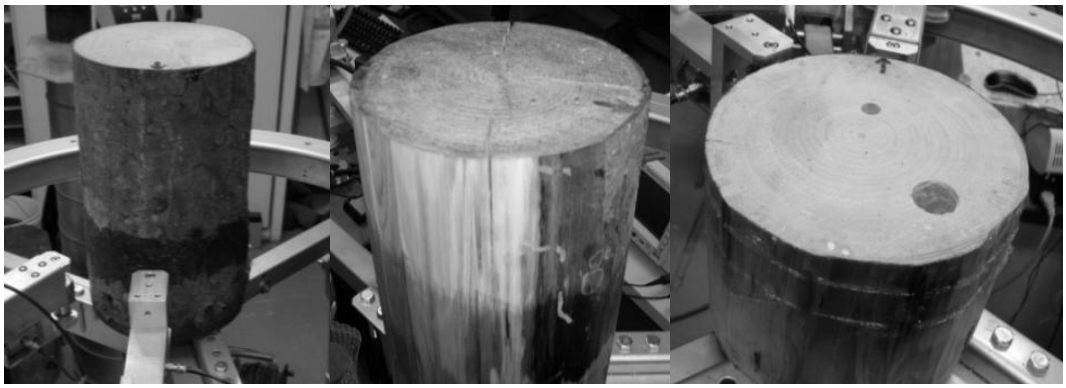

Figure 2. Tomography tests on the first log (from left to right: with bark, without bark and drilled with two holes measuring 1 cm and 2 cm in diameter).

The second log was cut into two 15-cm thick disks. The disks were taken from the middle section of the log. In one disk, a hole measuring 5 cm in diameter was drilled in the middle. In the other disk,

a hole measuring 5 cm in diameter was drilled off-centre (figure 3). The two disks underwent tomography testing with an angular step of 10°.

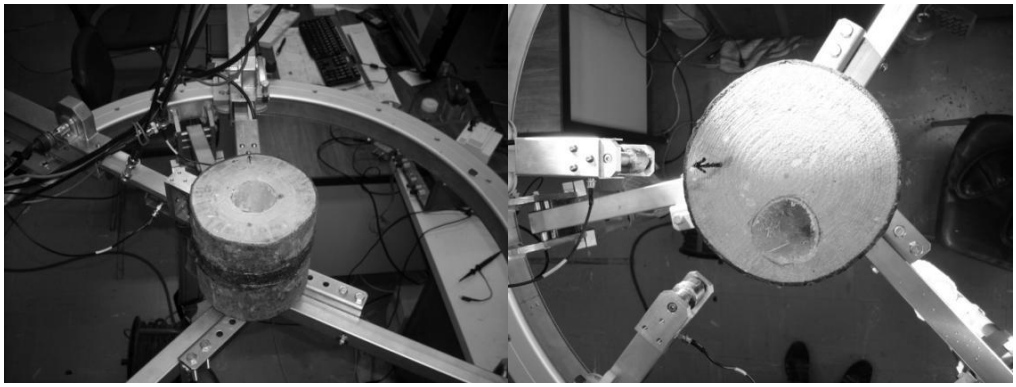

Figure 3. Tomography tests on the two disks of the second log (5-cm hole diameter).

2.3. Ultrasonic tomography

The ultrasonic tomograph used was an aluminium ring supported by a tripod (figure 4) [3]. In order to be able to test small disks, a specific support was added and mounted inside the tripod (figure 3). This device was designed to test standing trees. Thus, the height of the ring can be adjusted from 1 m to 1.6 m but the typical height is 1.3 m. If the apparatus is mounted on a trunk (figure 4) the two parts of the ring are first assembled, and then the tripod is fixed. The apparatus is then placed against the trunk using two narrowing elements. Each probe is mounted on a trolley and the trolleys are slid onto the ring. Finally, the last section of the ring is mounted and the third narrowing element is applied.

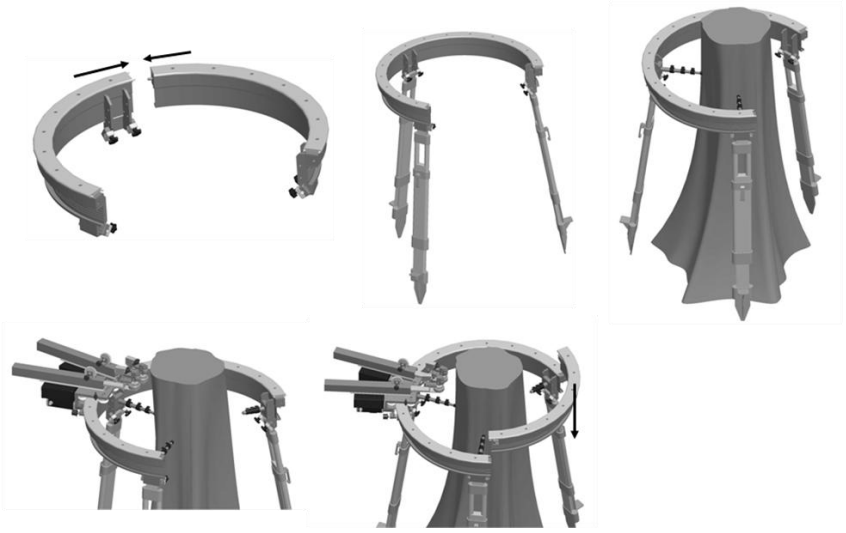

Figure 4. Assembly steps for the ultrasonic tomograph.

The probes had a frequency of 55 kHz and were designed for acoustic emission purposes. They were mounted on a specific support with a wheel, and grease was used as the coupling medium. Emission consisted in 5 square periods of 480 V. The output analog signal was amplified by 80 dB. Acquisition was via a converter with 16-bit resolution and a sampling frequency of 5 MHz. The acquisition time was set at 410 µs. The output signal was filtered beforehand by a Morlet wavelet at 55 kHz with a bandwidth of 20 kHz for denoising (figure 5).

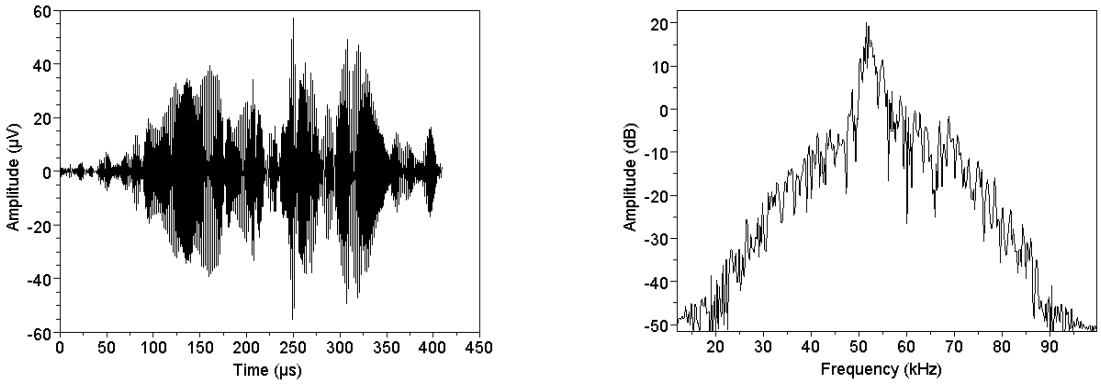

(a) (b)

Figure 5. Ultrasonic signal filtered by a Morlet wavelet at 55 kHz with a bandwidth of 20 kHz (a) and associated Fourier transform (b).

The ultrasonic parameters used for image reconstructions were slowness (s/m) and attenuation (dB/m at 55 kHz). Slowness, *Sl,* was computed using cross-correlation between the input and the output signals (equation 2). The ratio of received energy to emitted energy was used to determine attenuation *At* (equation 3).

$$Sl = \frac{1}{d} Max\left(\int e(s(-\tau)d\tau\right) \tag{2}$$

$$At = \frac{1}{d} 10\log_{10}\left(\frac{\int s^2(t)dt}{\int e^2(t)dt}\right) \tag{3}$$

where *Sl* is slowness, *At* attenuation, *d* the distance between the emitter and the receiver, *e(t)* the input signal and *s(t)* the output signal.

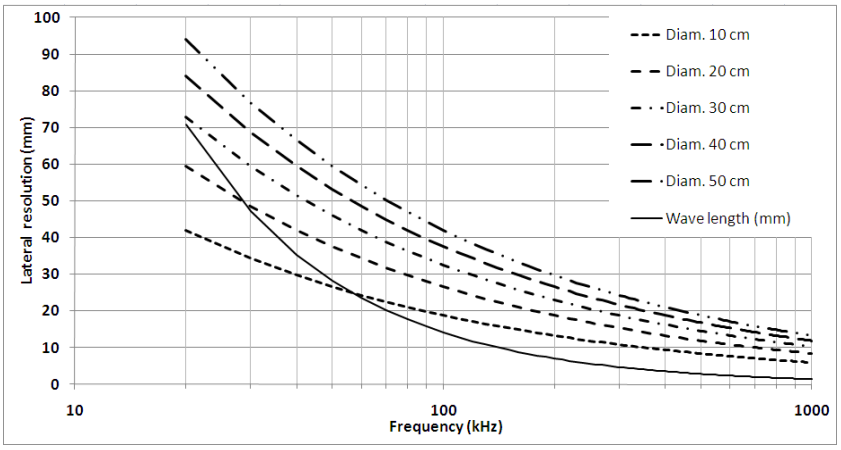

Figure 6. Lateral resolution and wavelength as a function of the frequency and depending on the sample diameter (the acoustic wave speed was set at 1400 m/s).

The tomographic images were computed using an angular step of 10°, which led to 900 acquisitions (36 equidistant acquisition points). A complete scan was completed in 40 minutes with the apparatus. In comparison, three well-trained operators were asked to carry out their own scan with 18 measurement points (306 acquisitions) and the duration of the scanning process was never less than one hour.

For a projection, the emitter remained motionless while the receiver moved around the ring. The next projection was initiated by an angular step motion of the emitter followed by another motion of the receiver all the way around the ring (acquisition took place on each angular step). The reconstruction algorithm used was based on the inverse Radon transform in fan beam geometry (linear interpolation) with a modified Shepp-Logan filter. Considering the medium to be isotropic, the elastic waves were assumed to propagate in a straight line. The velocity (and therefore the attenuation) of waves was then obtained by measuring travel-time (of energy) differences by inverting the Radon transform.

The theoretical upper limit of the number of computed pixels was 450 (mesh of 39 mm², equation 4). However, the physical resolution was about 26 mm (axial resolution: wavelength) and 31 mm (lateral resolution: Fresnel zone, equation 5, figure 6). This resolution led to a mesh of 806 mm²; the images were thus 2D smoothed by a Blackman filter of the wavelength size (the errors induced by the use of the modified Shepp-Logan filter were also greatly reduced). It is important to point out that the redundancy of the information (39 mm² compared to 806 mm²) made it possible to decrease the effect of erroneous experimental values in the imaging process.

$$N_{Pixels} = \frac{N_{Projections} \times N_{Sample}}{2} \tag{4}$$

where N_{Pixels} is the number of pixels, $N_{Projections}$ the number of projections (36) and N_{Sample} the number of acquisitions per projection (25).

$$R_F = \sqrt{\frac{S_d C}{2 f}} \tag{5}$$

where R_F is the Fresnel zone radius, S_d the scanned depth (the rotation radius of the emitter or receiver transducer), C the wave celerity and f the frequency of the transducer.

3. Results and discussion

In the following paragraphs, slowness is presented in 10^3 (s/m) or its inverse, speed in (m/s). Attenuation (in dB/m) was normalized by the diameter and thus presented in (dB).

3.1. Moisture content determination

The mean moisture content was 23% before the tests and 21% at the end of the experiment. The moisture content profile along the radius is presented in figure 7. The difference in moisture content from the pith to the bark was 5% before the test and 10% after the test. Despite the logs and disks being wrapped in plastic film, the wood samples tested were not in a green state and the natural drying effect increased while testing (a major phenomenon after bark removal). Small cracks appeared around the edge of the disks due to drying (figure 2, right-hand image).

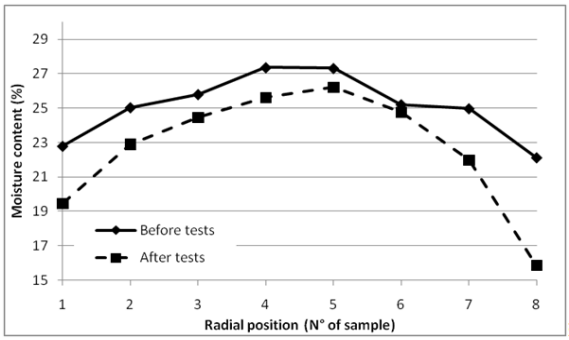

Figure 7. Moisture content (%) depending on the radial position before and after the ultrasonic tests (samples from the first log).

3.2. Measurement uncertainties

Two tomography tests were conducted with an angular step of 30° (108 acquisitions) on the same disk (with bark, without bark and drilled). The results are shown in figure 8 for the disk with bark only, as the trends were very similar after bark removal and drilling. Significant linear relationships were found for speed ($R^2 = 0.54$, $F = 105$, $p < 0.001$, $N = 108$) and for attenuation ($R^2 = 0.93$, $F = 1373$, $p < 0.001$, $N = 108$). The presence of outliers in the scatter plots for speed (figure 8, a) was caused by errors in the travel time estimation. The standard error of speed determination was thus ±420 m/s. Attenuation had a low measurement error compared to the speed estimation, with a standard error equal to ±1.7 dB.

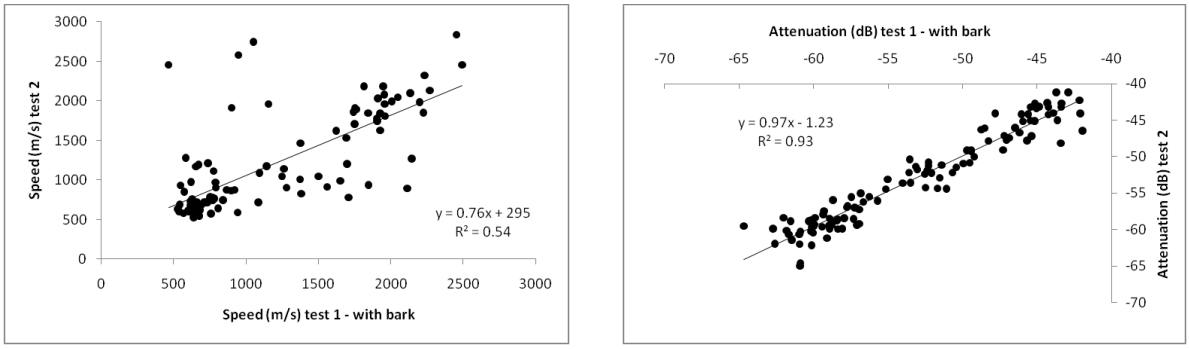

(a) (b)

Figure 8. Relationship between the two replications for (a) speed and (b) attenuation (disk with bark, N=108).

In actual practice, defects detection in trees like fungal decay depends on the ability of measuring acoustic impedance variations. It was reported that the weight loss due to fungal activity was linked to the decrease of transverse acoustic velocity [13]. Taking into account the speed measurement error of the tomograph (±420 m/s), the threshold value of weight variation was computed and equal to 13%. A weight loss of 13% is thus linked to the minimum variation of velocity detectable by the tomograph. This threshold can be associated to a moderate degradation state of the material.

3.3. Effect of bark and holes on the ultrasonic parameters

Mean comparisons were made to examine how bark and holes affected the ultrasonic parameters (figure 9). There were 108 acquisitions with an angular step of 30°. The statistical tests were firstly a

Student's t-test on paired samples (table 1). The *t*-test provides an exact test for the equality of the means of two normal populations with unknown, but equal, variances. The test statistic is based on a Student's distribution *t* with the degrees of freedom *d.f.* (table 1). The associated *p*-value is the probability that the means are the same.

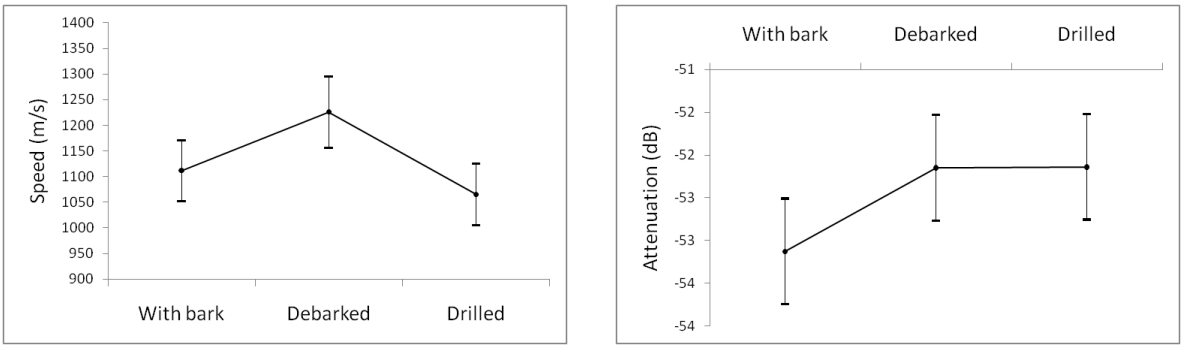

(a) (b)

Figure 9. Means and standard deviations of speed (a) and attenuation (b) computed on 108 acquisitions for the disk with bark, without bark and drilled.

Table 1. *t*-Test and Wilcoxon test on paired samples for speed and attenuation between the disk with bark, without bark and drilled.

Data sets	**t**	**d.f.**	***p*-value (bilateral)**	**Wilcoxon *p* (bilateral)**
With bark - without bark				
Speed	-1.934	107	0.056	0.496
Attenuation	-5.888	107	< 0.001	< 0.001
Drilled – Without bark				
Speed	2.196	107	0.030	0.126
Attenuation	-0.059	107	0.953	0.998

The *t*-test results, presented in table 1, were biased by the non-normal distribution of the parameters. To highlight this phenomenon, two histograms were plotted (figure 10) after the tomographic tests with an angular step of 10° (N=900). The bimodal distribution is shown in this figure for speed, with two modes between 1200 (m/s). The same type of distribution was also found for attenuation between -51 (dB). Equivalent findings were made for the disks without bark and the drilled disks.

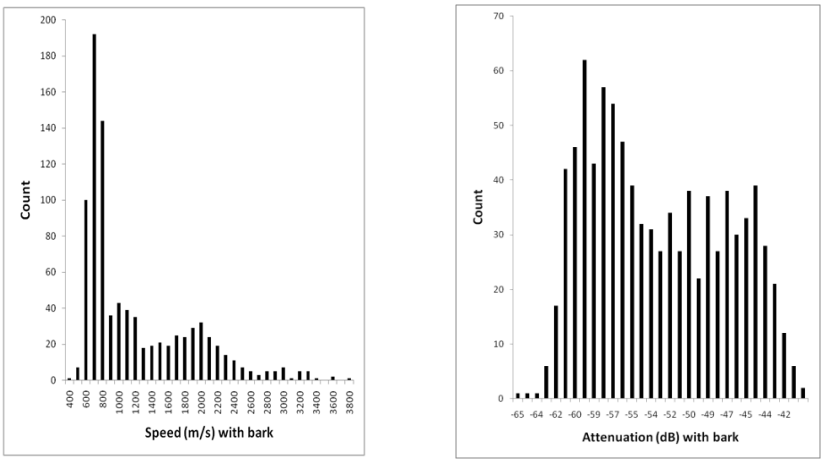

(a) (b)

Figure 10. Histograms of speed (a) and attenuation (b) of acoustic waves at 55 kHz computed for the disk with bark (N=900).

The results in table 1 were then completed by non-parametric Wilcoxon tests (valid when the normality assumption is not satisfied or the sample size is too small). The Wilcoxon tests agreed with those of the Student's t test for attenuation but did not confirm the Student's t results for speed (table 1). The mean attenuation measured on the disk with bark was thus significantly different from that for the disk without bark. The mean attenuation was higher with bark than without bark. No significant difference was found between the mean attenuation of the disk without bark and that of the drilled disk. For the speed measurements, differences existed between disks with bark, without bark and drilled disks, but the probability values were too high to be absolutely affirmative (figure 9 and table 1).

3.4. Relationship between slowness and attenuation

Figure 11 shows a scatter plot between slowness and attenuation for the disk with bark. A significant linear relationship was found with an R^2 equal to 0.51 ($F=933$, $p < 0.001$, $N=900$). Attenuation increased when slowness increased or speed decreased. However, the degree of fit should be read with care, as figure 11 clearly shows two populations (associated with the distributions of figure 10). Outliers were also visible due to the uncertainty of slowness determination, but they were not associated with particular positions of the probes.

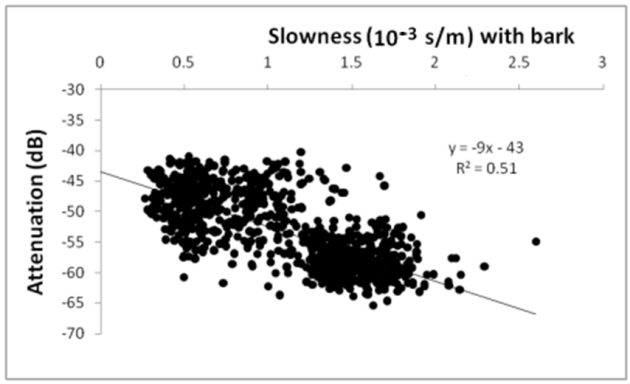

Figure 11. Relationship between slowness and attenuation for the disk with bark (N=900).

3.5. Tomographic images

The computed maps of slowness and attenuation for the first log with and without bark are presented in figure 12. The images were displayed in 87 x 87 pixels and based on a 10° angular step (900 acquisitions). There was no visible effect of the presence of bark on the outlines of the maps (figure 12). This phenomenon was due to the limited thickness of the bark (3 to 5 mm) compared to the wavelength (26 mm), combined with the smoothing effect of the 2D filter.

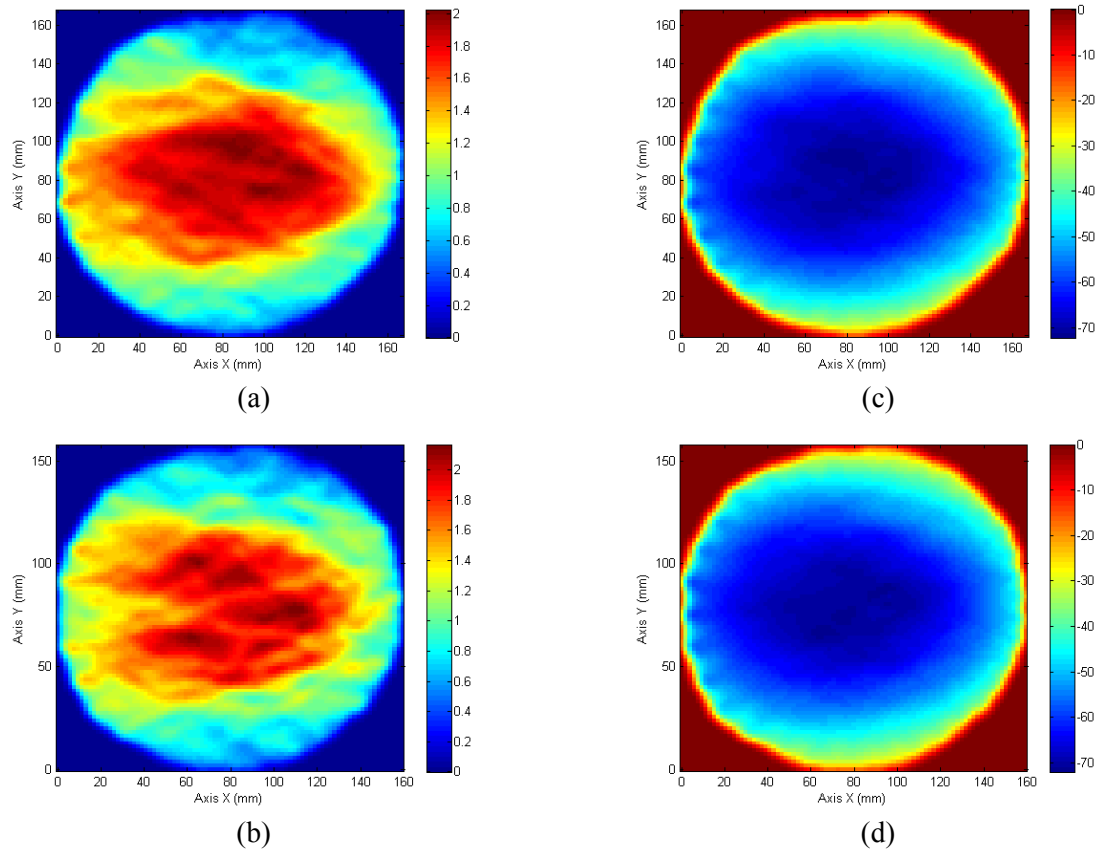

Figure 12. Tomographic maps of slowness (10^{-3} s/m) (a, b) and attenuation (dB) (c, d) for the disk of the first log, with bark (a, c) and without bark (b, d).

However, figure 12 shows two different areas from the pith to the periphery. These areas are highlighted in figure 13 in which the paths were drawn if slowness was lower than 1.2×10^{-3} s/m and if attenuation was over -51 dB. The periphery was thus characterized by higher speed and lower damping than those of the pith. The reverse phenomenon was found by Socco and interpreted as an effect of wood anisotropy [14]. The shorter paths (periphery) were more influenced by the tangential behaviour of wood, while the radial behaviour had a greater effect for longer paths (centre). However, the radial velocity of wood is known to be greater than the tangential velocity. In this specific case (figure 12), this observation was explained by the transition from juvenile to mature wood, combined with the effect of moisture distribution (figure 7).

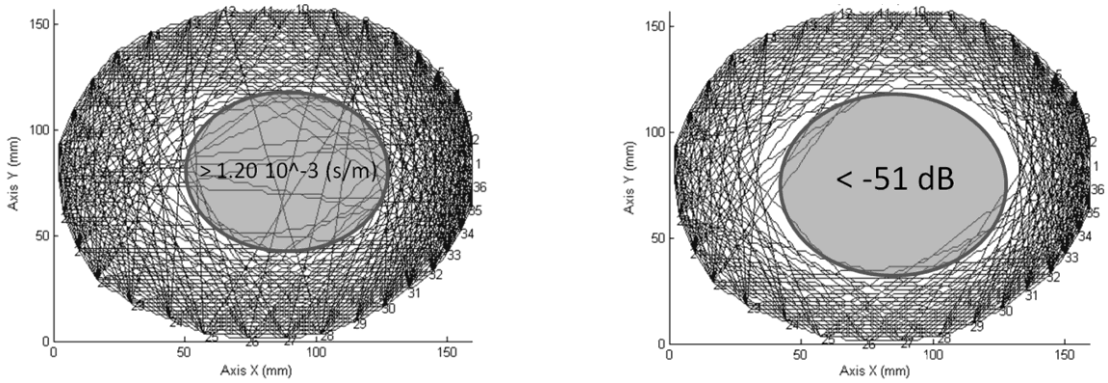

Figure 13. Paths from emitter to receiver with slowness under 1.2×10^{-3} s/m (a) and attenuation over -51 dB (b) for the disk of the first log with bark.

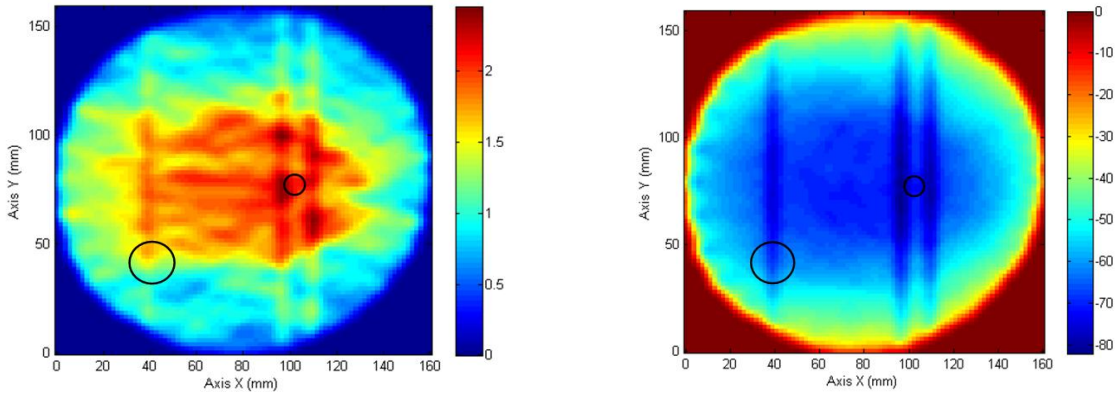

Figure 14. Tomographic maps of slowness (10^{-3} s/m) (a) and attenuation (dB) (b) for the drilled disk of the first log. The black circles indicate the positions of the drillings.

The tomographic images obtained for the drilled disks of the two logs are presented in figure 14 and figure 15. The effect of the holes can be seen on the maps by areas with high slowness and also high damping. This observation was valid even for the hole with a diameter (10 mm) half that of the wavelength (26 mm). It seems that the position of the holes in the disk had an effect on the reconstructed pattern; the holes close to the pith were characterized by two elliptic patterns unlike those close to the periphery. The shape of the patterns associated with the holes was not a circle but an ellipse and several hypotheses were advanced: anisotropy was not taken into account, some cracks due to natural drying occurred, the reconstruction procedure was not well adapted for missing data (the dimension of the probe supports did not enable scanning of the total angular area but only 250° for each projection), the mounting of the probes (figure 5, right-hand image) induced back-waves which altered the received signals. These hypotheses will be investigated in a future study to improve the tomographic process.

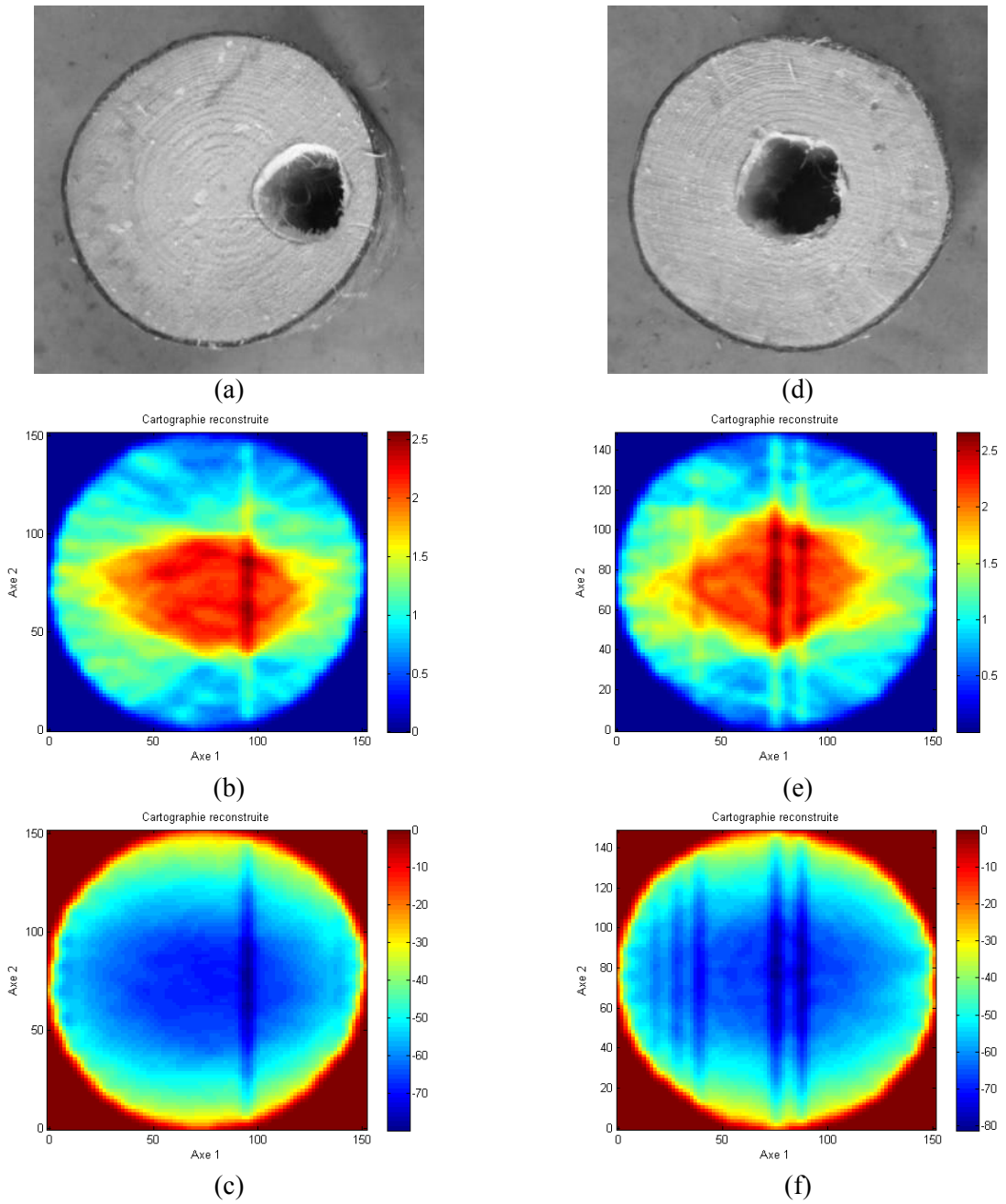

Figure 15. Tomographic maps of slowness (10^{-3} s/m) (b, e) and attenuation (dB) (c, f) for the two disks of the second log (a, b).

4. Conclusions

An automatic tomograph device specifically designed for standing trees is presented. The scanning process employed constitutes an improvement compared to previous work. This improvement has resulted in a fast process with only two probes giving scans with an angular precision of 10 degrees without any intervention by an operator during the process. This tomograph was used on two spruce (*Pica abies*) logs to study the effect of bark, and also the effect of defects, such as holes, on the reconstructed images. The tests were not carried out in the green state, but with a mean moisture content of 22% and a gradient of 7% between the pith and the periphery. The ultrasonic parameters

used for wood imaging were slowness and attenuation. The use of attenuation has not been reported in earlier work and its determination was found to be more accurate compared to that of slowness. Time of flight determination was found to be less accurate, even when cross-correlation was employed. This phenomenon was due to the dispersion and dissipation of wood material, leading to high attenuation combined with modifications in the incident waves. The means of the ultrasonic parameters were not sufficient for determining the existence of defects in trees, but the presence of bark significantly contributed to signal attenuation. For the test samples, it was shown that speed near the bark was greater than in the pith, due to the existence of juvenile wood, combined with the moisture gradient (natural drying occurred during the tests). Likewise, damping near the bark was lower than in the centre. A significant relationship was shown between slowness and attenuation, but the population was bimodal due to the presence of juvenile wood. However, it was possible to see that a high speed was coherent with low damping. The presence of bark was not visible on the tomographic images. This was probably due to its limited thickness compared to the wavelength. However, the presence of holes was clearly visible, but artifacts prevented precise shape reconstruction and location. Removing those artifacts will be the objective of future work.

5. Acknowledgments

The BIOGMID project was supported by a grant from the French National Research Agency (BLAN07-1_183692, “BioGMID”).

References

[1] Barnett J and Jeronimidis G 2003 *Wood Quality and its Biological Basis* (Oxford: Blackwell)
[2] Beall F C 2002 *Wood Sci. Technol.* **36** 197–212
[3] Brancheriau L, Gallet P, Thaunay P and Lasaygues P 2009 *6th Plant Biomechanics Conf.* 285-88
[4] Bucur V 2003 *Meas. Sci. Technol.* **14** 91-8
[5] Deflorio G, Fink S and Schwarze F 2008 *Wood Sci. Technol.* **42** 117–32
[6] Dikrallah A, Kabouchi B, Hakam A, Brancheriau L, Baillères H, Famiri A and Ziani M 2010 *C. R. Mecanique* **338** 107-12
[7] Divos F and Divos P 2005*14th Int. Symp. on Nondestructive Testing of Wood* 309-14
[8] Lin C, Kao Y and Lin T , Tsai M, Wang S, Lin L, Wang Y and Chan M 2008 *Int. Biodeterioration & Biodegradation* **62** 434-41
[9] Maurer H R, Schubert S, Baechle F, Clauss S, Gsell D, Dual J, and Niemz P 2006 *Holzforschung* **60** 567–73
[10] Nicolotti G, Socco L V, Martinis R, Godio A and Sambuelli L 2003 *Journal of Arboriculture* **29** 66–78
[11] Rinn F 2004 *Neue Landschaß* **7** 44-7
[12] Schmoldt D L 1996 *24th Annual Hardwood Symp.* 69-80
[13] Schubert S 2007 *Acousto-ultrasound assessment of inner wood decay in standing trees: possibilities and limitations* (Zürich: Diss ETH #17126)
[14] Socco L V, Sambuelli L, Martinis R, Comino E and Nicolotti G 2004 *Research in Nondestructive Evaluation* **15** 31-54
[15] Wang X, Allison R B, Wang L and Ross R J 2007 *U.S. Forest Products Laboratory* FPL-RP-642
[16] Wang X, Divos F, Pilon C, Brashaw B K, Ross R J and Pellerin R F 2004 *U.S. Forest Products Laboratory* FPL-GTR-147
[17] Wang X, Wiedenbeck J, Ross R J, Forsman J W, Erickson J R, Pilon C and Brashaw B K 2005 *U.S. Forest Products Laboratory* FPL–GTR–162